Electronic Supplementary Material (ESI) for Journal of Materials Chemistry A.

Supporting Information

Charting the Electronic Structure for Discovering Low-cost Intermetallic Catalysts

Zhengda He[1], Bin Ouyang[1,*]

[1]Department of Chemistry and Biochemistry, Florida State University, Tallahassee, FL 32304, USA.

1 Three-dimensional voxel plot for the number of surfaces of ternary intermetallics

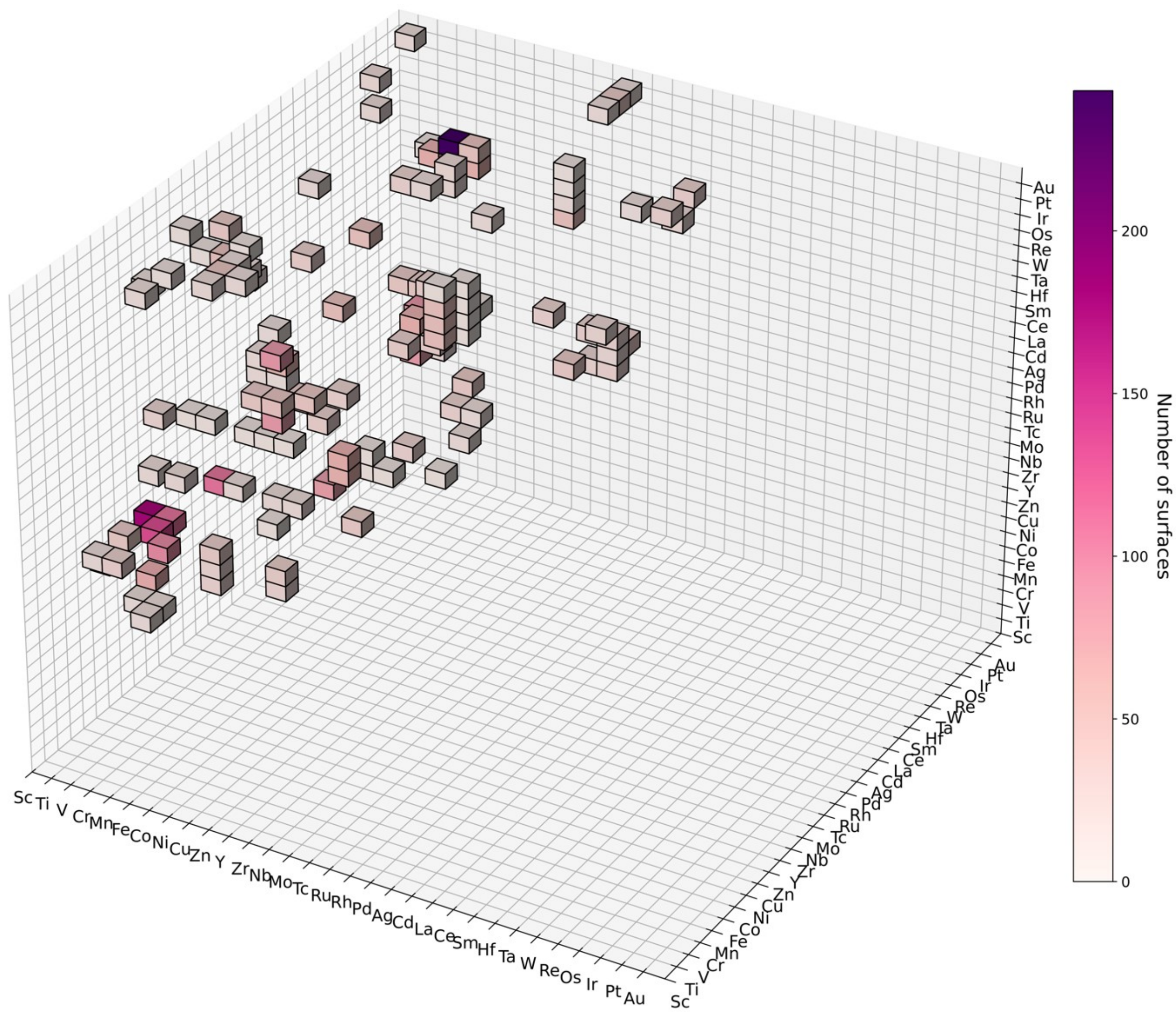

Figure S1. 3D voxel plot for illustrating the count of surfaces for each ternary composition. All compositions are sorted according to the atomic number of each element.

2 Calculating thermodynamic overpotential for HER and ORR

The mechanisms for HER and ORR used in this work are:

- HER
    - Step 1: $H^+ + e^- + * \rightarrow H_{ads}$
    - Step 2: $H_{ads} + H^+ + e^- \rightarrow H_2 + *$
- ORR
    - Step 1: $O_2 + H^+ + e^- + * \rightarrow OOH_{ads}$
    - Step 2: $OOH_{ads} + H^+ + e^- \rightarrow O_{ads} + H_2O$
    - Step 3: $O_{ads} + H^+ + e^- \rightarrow OH_{ads}$
    - Step 4: $OH_{ads} + H^+ + e^- \rightarrow H_2O + *$

The adsorption energies of intermediates (H/O/OH/OOH), denoted as $\Delta G^{H/O/OH/OOH}_{ads}$, are calculated by the free energy of following reactions:

- H_{ads} : $H^+ + e^- + * \rightarrow H_{ads}$
- O_{ads} : $H_2O + * \rightarrow O_{ads} + 2H^+ + 2e^-$
- OH_{ads} : $H_2O + * \rightarrow OH_{ads} + H^+ + e^-$
- OOH_{ads}: $2H_2O + * \rightarrow OOH_{ads} + 3H^+ + 3e^-$

The free energy (G) is calculated by: $G = E + ZPE - T \times S$, where ZPE and $T \times S$ are the zero-point energy and entropy contribution. The values of ZPE and $T \times S$ for reference (H_2, H_2O) and adsorbates ($H_{ads}/O_{ads}/OH_{ads}/OOH_{ads}$) are adopted from Ref 1 and 2.

Computational hydrogen electrode (CHE) was used to estimate the free energy of proton-electron pair ($G(H^+) + G(e^-)$) at different pH and electrode potential[2]. In this work pH was set to be 0. H_2 and H_2O were used as reference states.

Overpotentials of HER and ORR are calculated using the most positive free energy of elementary steps at the equilibrium electrochemical potential, 0V for HER and 1.23V for ORR. The overpotentials of HER (η_{HER}) and ORR (η_{ORR}) are calculated by:

$$\eta_{HER} = \max\left(\Delta G_1^{HER}, \Delta G_2^{HER}\right)/e_0$$

$$\eta_{ORR} = \max\left(\Delta G_1^{ORR}, \Delta G_2^{ORR}, \Delta G_3^{ORR}, \Delta G_4^{ORR}\right)/e_0$$

3 Formulation for DOS-shape descriptors

Here are the mathematical formulations for all five DOS-shape descriptors. We use $\rho(E)$ to represent the density of states, E_{min} and E_{max} represent the lowest and highest value of energy. All energies are referenced to the Fermi level ($E_F = 0eV$).

The formula for calculating d-band center (denoted as d_c) is:

$$d_c = \frac{\int_{E_{min}}^{E_{max}} E\rho(E)dE}{\int_{E_{min}}^{E_{max}} \rho(E)dE}$$

The formula for calculating d-band width (denoted as d_w) is:

$$d_w = \sqrt{\frac{\int_{E_{min}}^{E_{max}} (E - d_c)^2 \rho(E)dE}{\int_{E_{min}}^{E_{max}} \rho(E)dE}}$$

The formula for calculating d-band skewness (denoted as d_s) is:

$$d_s = \frac{\int_{E_{min}}^{E_{max}} (E - d_c)^3 \rho(E) dE}{\int_{E_{min}}^{E_{max}} \rho(E) dE} * \left(\frac{\int_{E_{min}}^{E_{max}} \rho(E) dE}{\int_{E_{min}}^{E_{max}} (E - d_c)^2 \rho(E) dE} \right)^{\frac{3}{2}}$$

The formula for calculating d-band kurtosis (denoted as d_k) is:

$$d_k = \frac{\int_{E_{min}}^{E_{max}} (E - d_c)^4 \rho(E) dE}{\int_{E_{min}}^{E_{max}} \rho(E) dE} * \left(\frac{\int_{E_{min}}^{E_{max}} \rho(E) dE}{\int_{E_{min}}^{E_{max}} (E - d_c)^2 \rho(E) dE} \right)^{2}$$

The formula for d-upper edge (denoted as d_u) is (from Ref. 3):

$$d_u = \underset{E}{\mathrm{argmax}} \frac{1}{\pi} P \int_{-\infty}^{+\infty} \frac{\rho(E')}{E - E'} dE'$$

4 Distribution of DOS-shape descriptors on all elements

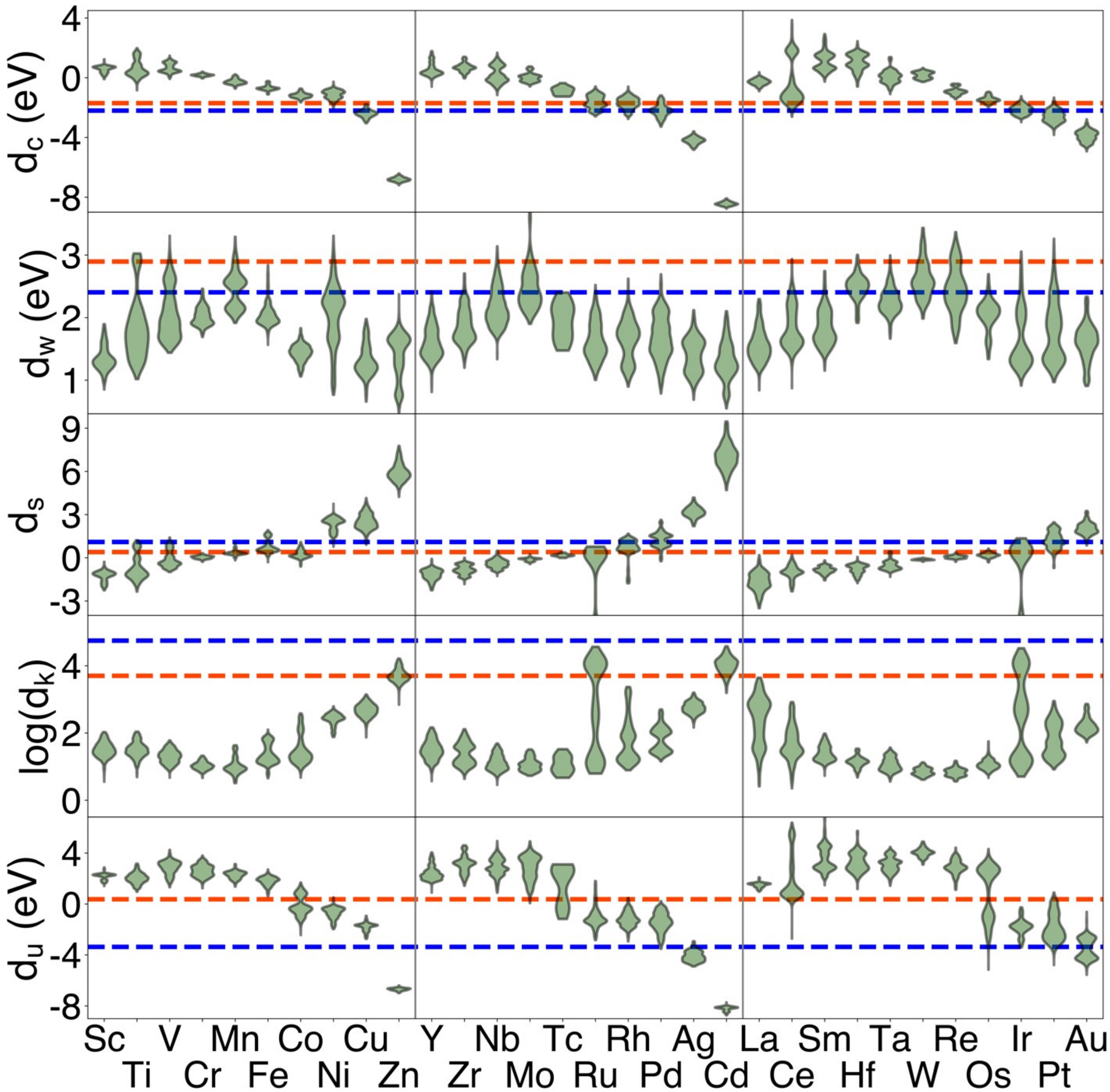

Figure S2. The violin plot for the distribution of the five DOS-shape descriptors. The blue and orange dashed lines represent the value of the descriptor for surface site at Pt(111) and Ir(111), respectively.

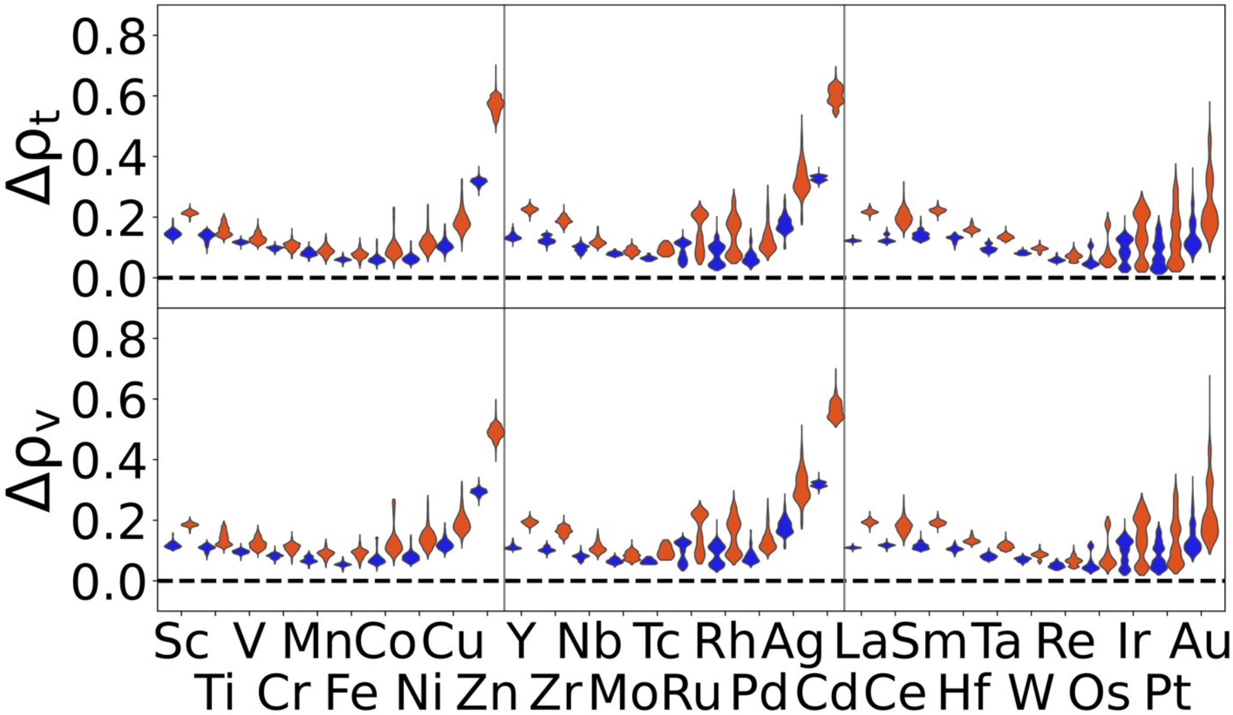

Figure S3. The violin plot for the distribution of the both DOS-similarity descriptors. The blue and orange represent the value of the descriptor calculated by reference to the surface site of Pt(111) and Ir(111), respectively.

5 Selecting promising sites from noble-metal-contained (NC) pool

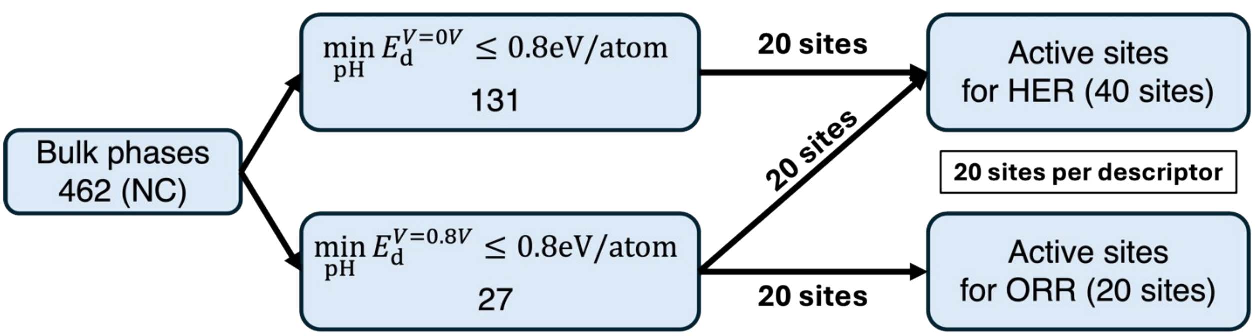

Figure S4. Workflow for selecting top promising sites for HER and ORR when considering noble-metal-contained pools. In total we have 40 sites for HER and 20 sites for ORR per descriptor.

5.1 Considering stable bulk phases in HER condition.

Table S1. Top three candidates selected by using single-site (ss) descriptors (δ_{ss}) comparing with reference sites (Ir/Pt). All bulk phases are stable under HER condition.

		1st candidate			2nd candidate			3rd candidate		
Ref	δ	Material	(hkl)	Site	Material	(hkl)	Site	Material	(hkl)	Site

Pt	d_c	Pt_3Zn	(111)	Pt	$ZnCu_2Ni$	(120)	Cu	Pt_2FeCu	(102)	Pt
	d_w	Pt_6MnCr	(102)	Pt	$PdFe$	(120)	Fe	Pt_6FeNi	(110)	Fe
	d_{skew}	Pt_6FeNi	(102)	Pt	Pd_9ZrNb_2	(111)	Pd	Pd_3Nb	(211)	Pd
	d_{kurt}	Pd_3Nb	(112)	Pd	Pd_3Nb	(012)	Pd	Pd_3Nb	(210)	Pd
	d_{up}	Ag_2CdZn	(211)	Ag	$PtMo_3$	(100)	Pt	$CuAu$	(112)	Au
	$\Delta\rho_{tot}$	Pt_6FeNi	(112)	Pt	Pt_6FeNi	(211)	Pt	Pt_6MnCr	(021)	Pt
	$\Delta\rho_{val}$	$CrIr_3$	(120)	Ir	$NbIr_3$	(221)	Ir	IrW	(211)	Ir
Ir	d_c	Cu_4Pd	(101)	Cu	Pt_3Mn	(112)	Pt	$PtCu_3$	(111)	Cu
	d_w	$Fe_{13}Co_3$	(211)	Fe	$Fe_{13}Co_3$	(112)	Fe	Ni_3Mo	(001)	Ni
	d_{skew}	Pt_3Sc	(111)	Pt	Pt_3Nb	(012)	Pt	Pd_3Fe	(120)	Fe
	d_{kurt}	$NbNi_6Mo$	(121)	Nb	$ZrNb_2Pd_9$	(111)	Zr	Pd_6MnFe	(111)	Fe
	d_{up}	Pt_3Zn	(120)	Pt	$PtNi$	(021)	Pt	$PtNi_3$	(110)	Pt
	$\Delta\rho_{tot}$	$CrIr_3$	(111)	Ir	Ir_3Os	(112)	Ir	IrW	(211)	Ir
	$\Delta\rho_{val}$	Ir_3Os	(112)	Ir	Ir_3Os	(110)	Ir	$CrIr_3$	(111)	Ir

5.2 Considering stable bulk phases in ORR condition.

Table S2. Top three candidates selected by using single-site (ss) descriptors (δ_{ss}) comparing with reference sites (Ir/Pt). All bulk phases are stable under ORR condition.

		1st candidate			2nd candidate			3rd candidate		
Ref	δ	Material	(hkl)	Site	Material	(hkl)	Site	Material	(hkl)	Site
Pt	d_c	Cu_3Au	(112)	Cu	Pt_3Co	(120)	Pt	$CuAu_3$	(100)	Cu
	d_w	Pt_3Ni	(120)	Pt	Pt_3Ni	(110)	Pt	Cu_3PdAu_4	(102)	Au
	d_{skew}	Pd_3Co	(110)	Co	Ag_3Pt	(110)	Pt	Pd_3Co	(120)	Co
	d_{kurt}	Pt_3Co	(111)	Pt	Pt_3Ni	(111)	Pt	Pd_3Co	(110)	Co
	d_{up}	Cu_3PdAu_4	(110)	Au	Pd_3Au	(111)	Au	$CdAu_3$	(100)	Au
	$\Delta\rho_{tot}$	Pt_3Ni	(111)	Pt	Pt_3Co	(111)	Pt	Pt_3Ni	(120)	Pt
	$\Delta\rho_{val}$	Pt_3Ni	(111)	Pt	Pt_3Co	(111)	Pt	Pt_3Co	(120)	Pt
Ir	d_c	Cu_3PdAu_4	(102)	Cu	Pt_3Ni	(120)	Pt	Cu_3Au	(120)	Cu
	d_w	Pt_3Ni	(111)	Pt	Cu_3Au	(100)	Au	Pt_3Co	(111)	Pt

	d_{skew}	Pt_3Co	(110)	Co	Pd_3Co	(110)	Co	Ag_3Pt	(120)	Pt
	d_{kurt}	Pt_3Co	(120)	Pt	Pt_3Ni	(100)	Ni	Pd_3Co	(110)	Co
	d_{up}	Pt_3Co	(120)	Pt	Pt_3Ni	(100)	Pt	Pd_3Co	(110)	Co
	$\Delta\rho_{tot}$	Pt_3Co	(111)	Pt	Pt_3Ni	(111)	Pt	Pt_3Co	(110)	Pt
	$\Delta\rho_{val}$	Pt_3Co	(111)	Pt	Pt_3Ni	(111)	Pt	Pt_3Co	(110)	Pt

6 Selecting promising sites from noble-metal-free pool (NF).

Table S3. Top three candidates selected by using single-site (ss) descriptors (δ_{ss}) comparing with reference sites (Ir/Pt).

		1st candidate			2nd candidate			3rd candidate		
Ref	δ	Material	(hkl)	Site	Material	(hkl)	Site	Material	(hkl)	Site
Pt	d_c	$ZnCu_2Ni$	(120)	Cu	Zn_2CuNi	(101)	Cu	Zn_2CuNi	(211)	Cu
	d_w	$NbNi_3$	(120)	Ni	$NbNi_6Mo$	(021)	Ni	$TaNi_6Mo$	(021)	Ni
	d_{skew}	$NbNi_3$	(011)	Nb	$NbNi_3$	(111)	Nb	$NbNi_3$	(221)	Nb
	d_{kurt}	$MnNi$	(100)	Mn	$NbCo_3$	(212)	Co	$CrFe_3$	(120)	Cr
	d_{up}	$ZnCu$	(110)	Cu	Zn_2CuNi	(120)	Cu	$ZnCu$	(111)	Cu
	$\Delta\rho_{tot}$	$NbCo_3$	(201)	Co	$NbCo_3$	(212)	Co	$CoNi_3$	(111)	Co
	$\Delta\rho_{val}$	$CoNi_3$	(100)	Co	$CoNi_3$	(110)	Co	$CoNi_3$	(111)	Co
Ir	d_c	$ZnCu_2Ni$	(211)	Cu	$ZnCu_2Ni$	(211)	Cu	$ZnCu_2Ni$	(101)	Cu
	d_w	$Fe_{13}Co_3$	(211)	Fe	$Fe_{13}Co_3$	(112)	Fe	Ni_3Mo	(001)	Ni
	d_{skew}	$TaNi_6Mo$	(021)	Ta	$TaNi_6Mo$	(100)	Ta	$NbNi_3$	(100)	Nb
	d_{kurt}	$NbNi_6Mo$	(121)	Nb	$NbNi_3$	(102)	Nb	$NbNi_3$	(111)	Nb
	d_{up}	Zn_3Co	(120)	Co	Fe_3Ni_2	(120)	Fe	Fe_3Ni_2	(120)	Fe
	$\Delta\rho_{tot}$	Fe_3Ni_2	(100)	Fe	Fe_3Ni_2	(100)	Fe	Fe_3Ni_2	(101)	Fe
	$\Delta\rho_{val}$	Fe_3Ni_2	(100)	Fe	Fe_3Ni_2	(100)	Fe	$FeNi_3$	(111)	Fe

7 Promising candidates for HER and ORR in NC and NF pools

Important details are also shown in the table: the descriptor and references (Pt/Ir) used to predict the catalyst along with the corresponding values, the composition and Miller index of the surface, the overpotential for HER/ORR and decomposition energies at reaction condition, the corresponding literature if the catalyst was reported before. We only listed the references for non-Pt catalysts since Pt was a common choice for HER and ORR catalysts, N/A represents no literature have been found on the corresponding composition.

Table S4. Promising surfaces for HER ($\eta_{HER} \leq 0.3\ V$) and ORR ($\eta_{ORR} \leq 0.8\ V$) predicted from noble-metal-containing pool.

Hydrogen Evolution Reaction							
Ref	**Metric**	**Value/Ref**	**Composition**	**Miller**	η_{HER} **(V)**	E_{decomp}^{min} **(eV)**	**Report**
Pt	d_c	-1.93/-1.94	$MnCrPt_6$	(112)	0.001	0.21	N/A
Pt	d_k	4.75/4.75	$ZnPt_3$	(111)	0.002	0.00	
Ir	$\Delta\rho_t$	0.02/0.00	$CrIr_3$	(111)	0.002	0.20	N/A
Ir	d_u	0.35/0.37	$NiPt_3$	(120)	0.003	0.00	
Ir	d_s	0.90/0.62	Ag_3Pt	(120)	0.007	0.00	
Ir	$\Delta\rho_v$	0.03/0.00	Ir_3Os	(111)	0.012	0.00	N/A
Pt	d_u	-3.31/-3.37	Mo_3Pt	(112)	0.015	0.42	
Pt	d_c	-1.93/-1.94	$FeCuPt_2$	(102)	0.025	0.05	
Pt	d_k	4.72/4.75	$NbPd_3$	(210)	0.026	0.46	N/A
Ir	d_s	0.60/0.62	$ScPt_3$	(111)	0.028	0.38	N/A
Pt	d_w	2.34/2.40	$FeCoPt_2$	(021)	0.029	0.14	N/A
Ir	d_u	-0.22/0.37	NiPt	(021)	0.031	0.00	
Pt	$\Delta\rho_t$	0.01/0.00	$FeNiPt_6$	(112)	0.038	0.00	
Ir	d_c	-1.80/-1.77	MoIr	(112)	0.064	0.00	4
Pt	d_c	-1.97/-1.94	$MnPt_3$	(111)	0.068	0.00	
Pt	$\Delta\rho_v$	0.04/0.00	$NbIr_3$	(211)	0.075	0.22	N/A

Ir	d_u	0.40/0.37	$CoNiPt_2$	(021)	0.080	0.00	
Ir	$\Delta\rho_v$	0.05/0.00	$CoPt_3$	(112)	0.091	0.00	
Ir	d_u	-0.83/0.37	$NbRh_3$	(201)	0.098	0.29	N/A
Ir	d_s	0.52/0.62	$TaRh_3$	(111)	0.109	0.45	N/A
Pt	d_k	4.91/4.75	VPt	(211)	0.115	0.40	N/A
Pt	d_w	2.34/2.40	$NbPt_2$	(001)	0.124	0.34	N/A
Ir	d_k	3.45/3.70	MoPt	(001)	0.133	0.00	
Ir	d_w	2.87/2.90	$MnNi_3$	(111)	0.148	0.11	5
Ir	d_k	3.51/3.70	IrW	(011)	0.265	0.00	6
Pt	d_w	2.39/2.40	$NbNi_3$	(120)	0.298	0.27	N/A

Oxygen Reduction reaction

Ref	Metric	Value	Bulk	Miller	η_{ORR} (V)	E_{decomp}^{min} (eV)	Report
Pt	d_w	2.42/2.40	Cu_3Au	(112)	0.41	0.53	7
Pt	d_u	0.12/0.62	$CdAu_3$	(100)	0.43	0.81	N/A
Ir	d_c	-2.68/-3.37	$CuAu_3$	(112)	0.52	0.26	7
Ir	$\Delta\rho_v$	-1.78/-1.77	$CoPt_3$	(110)	0.54	0.12	
Pt	d_u	-3.25/-3.37	Pd_3Au	(112)	0.57	0.06	8
Pt	d_s	1.01/0.62	Ag_3Pt	(100)	0.58	0.00	
Ir	d_c	-1.84/-1.77	Cu_3PdAu_4	(102)	0.65	0.09	N/A
Pt	$\Delta\rho_t$	0.03/0.00	$NiPt_3$	(110)	0.69	0.12	

Table S5. Promising surfaces for HER ($\eta_{HER} \leq 0.3\ V$) and ORR ($\eta_{ORR} \leq 0.8\ V$) predicted from noble-metal-free pool.

Hydrogen Evolution Reaction

Ref	Metric	Value	Bulk	Miller	η_{HER} (V)	E_{decomp} (eV)	Report
Pt	d_k	4.81/4.75	$NbCo_3$	(212)	0.022	0.73	9,10
Ir	d_k	3.69/3.70	$NbNi_3$	(111)	0.124	0.48	N/A
Ir	d_u	0.34/0.37	Zn_3Co	(120)	0.200	0.26	11

Pt	d_w	2.27/2.40	$TaNi_6Mo$	(021)	0.241	0.26	N/A
Ir	d_w	2.68/2.90	Ni_3Mo	(001)	0.291	0.00	12
Pt	$\Delta\rho_v$	0.06/0.00	$CoNi_3$	(111)	0.297	0.00	N/A
Oxygen Reduction Reaction							
Ref	**Metric**	**Value**	**Bulk**	**Miller**	η_{ORR} **(V)**	E_{decomp} **(eV)**	**Report**
Pt	d_u	-2.51/-3.37	ZnCu	(110)	0.56	1.20	13
Pt	d_u	-2.32/-3.37	Zn_2CuNi	(120)	0.67	1.05	N/A
Ir	d_c	-1.86/-1.77	$ZnCu_2Ni$	(211)	0.75	0.59	N/A

8 Promising sites for HER and ORR --- Complete data

In this section we showed the bulk phases, miller indexes and sites for all promising active sites for HER and ORR using NC and NF pools. We have omitted the indexes of miller surfaces (some miller index will have multiple surfaces with different index) and chosen three decimal points for η_{HER}. This will cause duplications in the table, but in fact each row represents a unique active site. This is also the case for Table S7-7.

8.1 Active sites for HER using NC pool

Table S6. Promising candidates for HER using NC pool sorted by the overpotential of HER (η_{HER}). Only the sites with $\eta_{HER} \leq 0.3V$ (considered successful predictions in this work) have been shown. The symbols for the descriptors are: (1) d-band center (d_c) (2) d-band width (d_w) (3) d-band skewness (d_s) (4) d-band kurtosis (d_k) (5) d-band upper edge (d_u) (6) total-DOS similarity ($\Delta\rho_t$) (7) valence-DOS similarity ($\Delta\rho_v$). $E_{decomp,min}^{@E_{HER}^0-\eta_{HER}}$ represents the minimal decomposition energy of bulk phases at potential $U = E_{HER}^0 - \eta_{HER}$ across pH from 0 to 14, $E_{HER}^0 = 0$V is the standard equilibrium potential of HER.

Ref	Descriptor	Bulk	Miller Index	Site	η_{HER} (V)	$E_{decomp,min}^{@E_{HER}^0-\eta_{HER}}$ (eV)
Pt	d_c	$MnCrPt_6$	(112)	Pt	0.001	0.21

Pt	d_c	$MnCrPt_6$	(112)	Pt	0.001	0.24
Pt	d_k	Pt_3Zn	(111)	Pt	0.002	0.00
Ir	$\Delta\rho_t$	$CrIr_3$	(111)	Ir	0.002	0.20
Ir	$\Delta\rho_t$	$CrIr_3$	(111)	Ir	0.002	0.20
Ir	d_u	$NiPt_3$	(120)	Pt	0.003	0.00
Pt	$\Delta\rho_t$	$NiPt_3$	(120)	Pt	0.003	0.00
Pt	$\Delta\rho_v$	$NiPt_3$	(120)	Pt	0.003	0.00
Pt	d_w	$NiPt_3$	(120)	Pt	0.003	0.00
Ir	d_c	$NiPt_3$	(120)	Pt	0.003	0.00
Ir	d_s	Ag_3Pt	(120)	Pt	0.007	0.00
Pt	d_s	Ag_3Pt	(120)	Pt	0.007	0.00
Pt	d_s	Ag_3Pt	(110)	Pt	0.009	0.02
Ir	d_s	Ag_3Pt	(110)	Pt	0.009	0.00
Ir	$\Delta\rho_v$	Ir_3Os	(111)	Os	0.012	0.00
Pt	d_u	Mo_3Pt	(112)	Pt	0.015	0.42
Pt	d_u	Mo_3Pt	(100)	Pt	0.020	0.41
Pt	d_u	Mo_3Pt	(112)	Pt	0.022	0.27
Pt	d_c	$FeCuPt_2$	(102)	Pt	0.025	0.05
Pt	d_k	$NbPd_3$	(210)	Pd	0.026	0.46
Pt	d_c	$MnCrPt_6$	(112)	Pt	0.027	0.23
Pt	d_c	$MnCrPt_6$	(112)	Pt	0.027	0.19
Ir	d_s	$ScPt_3$	(111)	Pt	0.028	0.38
Pt	d_w	$FeCoPt_2$	(021)	Pt	0.029	0.14
Ir	d_u	NiPt	(021)	Pt	0.031	0.00
Ir	d_u	NiPt	(120)	Pt	0.038	0.00
Pt	$\Delta\rho_t$	$FeNiPt_6$	(112)	Pt	0.038	0.00
Pt	$\Delta\rho_t$	$FeNiPt_6$	(112)	Pt	0.040	0.00
Pt	$\Delta\rho_t$	$FeNiPt_6$	(112)	Pt	0.046	0.00
Pt	$\Delta\rho_v$	$FeNiPt_6$	(112)	Pt	0.047	0.00

Pt	$\Delta\rho_t$	$FeNiPt_6$	(112)	Pt	0.047	0.00
Ir	$\Delta\rho_v$	$NiPt_3$	(111)	Pt	0.049	0.00
Ir	$\Delta\rho_t$	$NiPt_3$	(111)	Pt	0.049	0.00
Pt	$\Delta\rho_t$	$NiPt_3$	(111)	Pt	0.049	0.00
Ir	d_w	$NiPt_3$	(111)	Pt	0.049	0.00
Ir	d_k	$NiPt_3$	(111)	Pt	0.049	0.00
Pt	d_k	$NiPt_3$	(111)	Pt	0.049	0.00
Pt	d_c	$NiPt_3$	(111)	Pt	0.049	0.00
Pt	$\Delta\rho_v$	$NiPt_3$	(111)	Pt	0.049	0.00
Ir	$\Delta\rho_v$	$CrIr_3$	(111)	Ir	0.056	0.16
Ir	$\Delta\rho_t$	$CrIr_3$	(111)	Ir	0.056	0.16
Pt	$\Delta\rho_t$	$FeNiPt_6$	(211)	Pt	0.059	0.00
Ir	d_c	MoIr	(112)	Ir	0.064	0.00
Ir	d_u	$ZnPt_3$	(120)	Pt	0.065	0.00
Pt	$\Delta\rho_v$	$NiPt_3$	(110)	Pt	0.066	0.00
Pt	$\Delta\rho_t$	$NiPt_3$	(110)	Pt	0.066	0.00
Pt	d_w	$NiPt_3$	(110)	Pt	0.066	0.00
Ir	$\Delta\rho_t$	$NiPt_3$	(110)	Pt	0.066	0.00
Ir	d_c	$NiPt_3$	(110)	Pt	0.066	0.00
Pt	d_c	$MnPt_3$	(111)	Pt	0.068	0.00
Ir	d_s	Ag_3Pt	(100)	Pt	0.069	0.00
Pt	d_s	Ag_3Pt	(100)	Pt	0.069	0.02
Pt	$\Delta\rho_v$	$NbIr_3$	(211)	Ir	0.075	0.22
Pt	$\Delta\rho_v$	$NiPt_3$	(111)	Pt	0.080	0.00
Ir	$\Delta\rho_t$	$NiPt_3$	(111)	Pt	0.080	0.00
Ir	d_w	$NiPt_3$	(111)	Pt	0.080	0.00
Pt	d_c	$NiPt_3$	(111)	Pt	0.080	0.00
Pt	$\Delta\rho_t$	$NiPt_3$	(111)	Pt	0.080	0.00
Ir	$\Delta\rho_v$	$NiPt_3$	(111)	Pt	0.080	0.00

Pt	$\Delta\rho_t$	$NiPt_3$	(111)	Pt	0.080	0.00
Ir	$\Delta\rho_v$	$NiPt_3$	(111)	Pt	0.080	0.00
Ir	$\Delta\rho_t$	$NiPt_3$	(111)	Pt	0.080	0.00
Ir	d_u	$NiPt_3$	(111)	Pt	0.080	0.00
Ir	d_k	$NiPt_3$	(111)	Pt	0.080	0.00
Pt	$\Delta\rho_v$	$NiPt_3$	(111)	Pt	0.080	0.00
Pt	d_k	$NiPt_3$	(111)	Pt	0.080	0.00
Ir	d_w	$NiPt_3$	(111)	Pt	0.080	0.00
Ir	d_u	$CoNiPt_2$	(021)	Pt	0.080	0.00
Pt	$\Delta\rho_v$	$CrIr_3$	(120)	Ir	0.083	0.14
Ir	$\Delta\rho_v$	$CoPt_3$	(112)	Pt	0.091	0.00
Pt	$\Delta\rho_v$	$CoPt_3$	(112)	Pt	0.091	0.00
Ir	$\Delta\rho_t$	$CoPt_3$	(112)	Pt	0.091	0.00
Pt	d_w	$MnCrPt_6$	(102)	Pt	0.093	0.07
Ir	d_u	$NbRh_3$	(201)	Rh	0.098	0.29
Pt	$\Delta\rho_v$	$CrIr_3$	(110)	Ir	0.107	0.12
Ir	d_s	$TaRh_3$	(111)	Rh	0.109	0.45
Pt	d_k	VPt	(211)	Pt	0.115	0.40
Ir	$\Delta\rho_v$	Ir_3Os	(111)	Ir	0.118	0.00
Ir	$\Delta\rho_t$	Ir_3Os	(111)	Ir	0.118	0.00
Pt	$\Delta\rho_t$	$FeNiPt_6$	(112)	Pt	0.124	0.00
Pt	d_w	$NbPt_2$	(001)	Nb	0.124	0.34
Pt	$\Delta\rho_t$	$FeNiPt_6$	(112)	Pt	0.125	0.00
Pt	d_k	$NbPd_3$	(011)	Pd	0.125	0.34
Pt	d_k	$NbPd_3$	(011)	Pd	0.125	0.34
Ir	$\Delta\rho_v$	Ir_3Os	(110)	Ir	0.126	0.00
Ir	$\Delta\rho_t$	Ir_3Os	(110)	Ir	0.126	0.00
Ir	d_c	$MnCrPt_6$	(111)	Pt	0.126	0.27
Pt	d_s	$MnCrPt_6$	(111)	Pt	0.126	0.05

Ir	d_w	$NiPt_3$	(112)	Pt	0.126	0.00
Ir	$\Delta\rho_v$	$NiPt_3$	(112)	Pt	0.126	0.00
Ir	d_u	$NiPt_3$	(112)	Pt	0.126	0.00
Pt	d_w	$NiPt_3$	(112)	Pt	0.126	0.00
Ir	d_w	NiPt	(001)	Pt	0.127	0.00
Ir	$\Delta\rho_t$	Ir_3Os	(111)	Ir	0.128	0.00
Ir	$\Delta\rho_v$	Ir_3Os	(111)	Ir	0.128	0.00
Ir	$\Delta\rho_t$	Ir_3Os	(111)	Ir	0.128	0.00
Ir	$\Delta\rho_v$	Ir_3Os	(111)	Ir	0.128	0.00
Ir	d_k	MoPt	(001)	Mo	0.133	0.00
Ir	$\Delta\rho_t$	$CoPt_3$	(111)	Pt	0.137	0.00
Pt	d_s	$CoPt_3$	(111)	Pt	0.137	0.00
Pt	$\Delta\rho_v$	$CoPt_3$	(111)	Pt	0.137	0.00
Ir	$\Delta\rho_v$	$CoPt_3$	(111)	Pt	0.137	0.00
Ir	d_k	$CoPt_3$	(111)	Pt	0.137	0.00
Pt	$\Delta\rho_t$	$CoPt_3$	(111)	Pt	0.137	0.00
Ir	d_w	$CoPt_3$	(111)	Pt	0.137	0.00
Pt	d_k	$CoPt_3$	(111)	Pt	0.137	0.00
Ir	$\Delta\rho_t$	$CoPt_3$	(111)	Pt	0.137	0.00
Pt	$\Delta\rho_t$	$CoPt_3$	(111)	Pt	0.137	0.00
Ir	$\Delta\rho_v$	$CoPt_3$	(111)	Pt	0.137	0.00
Ir	d_w	$CoPt_3$	(111)	Pt	0.137	0.00
Pt	$\Delta\rho_v$	$CoPt_3$	(111)	Pt	0.137	0.00
Ir	d_k	$CoPt_3$	(111)	Pt	0.137	0.00
Ir	d_u	$MnCrPt_6$	(120)	Pt	0.146	0.04
Ir	$\Delta\rho_v$	Ir_3Os	(120)	Ir	0.148	0.00
Ir	d_s	$CoPt_3$	(110)	Pt	0.148	0.00
Pt	$\Delta\rho_t$	$CoPt_3$	(110)	Pt	0.148	0.00
Pt	d_c	$CoPt_3$	(110)	Pt	0.148	0.00

Ir	$\Delta\rho_t$	$CoPt_3$	(110)	Pt	0.148	0.00
Pt	d_k	$CoPt_3$	(110)	Pt	0.148	0.00
Ir	$\Delta\rho_v$	$CoPt_3$	(110)	Pt	0.148	0.00
Ir	d_k	$CoPt_3$	(110)	Pt	0.148	0.00
Pt	d_s	$CoPt_3$	(110)	Pt	0.148	0.00
Ir	d_w	$MnNi_3$	(111)	Ni	0.148	0.11
Pt	$\Delta\rho_v$	$NbIr_3$	(221)	Ir	0.160	0.11
Pt	d_c	$ZnPt_3$	(111)	Pt	0.173	0.00
Ir	d_c	$MnPt_3$	(112)	Pt	0.178	0.00
Ir	d_k	MoIr	(201)	Ir	0.194	0.00
Pt	d_w	MoPt	(021)	Pt	0.196	0.00
Pt	d_w	MoIr	(021)	Ir	0.206	0.00
Ir	$\Delta\rho_v$	Ir_3Os	(112)	Ir	0.234	0.00
Pt	$\Delta\rho_v$	Ir_3Os	(112)	Ir	0.234	0.00
Ir	$\Delta\rho_t$	Ir_3Os	(112)	Ir	0.234	0.00
Pt	d_w	$FeNiPt_6$	(110)	Fe	0.260	0.00
Ir	$\Delta\rho_t$	Ir_3Os	(100)	Ir	0.263	0.00
Ir	$\Delta\rho_v$	Ir_3Os	(100)	Ir	0.263	0.00
Pt	d_s	$NbPd_3$	(210)	Pd	0.263	0.18
Pt	d_s	$NbPd_3$	(210)	Pd	0.263	0.18
Ir	d_k	IrW	(011)	Ir	0.265	0.00
Pt	$\Delta\rho_v$	$CrIr_3$	(112)	Ir	0.295	0.00
Pt	d_w	NbNi3	(120)	Ni	0.298	0.27

8.2 Active sites for ORR using NC pool

Table S7. Promising candidates for ORR using NC pool sorted by the overpotential of ORR (η_{ORR}). Only the sites with $\eta_{ORR} \leq 0.8V$ (considered successful predictions in this work) have been shown. The symbols for descriptors are the same as Table S6. $E_{decomp,min}^{@E_{ORR}^{0}-\eta_{ORR}}$ represents the minimal decomposition energy of bulk phases at potential $U = E^0_{ORR} - \eta_{ORR}$ across pH from 0 to 14, $E^0_{ORR} = 0$V is the standard equilibrium potential of HER.

Ref	Descriptor	Bulk	Miller Index	Site	η_{ORR} (V)	$E_{decomp,min}^{@E^0_{ORR}-\eta_{ORR}}$ (eV)
Pt	d_w	Cu_3Au	(112)	Au	0.405	0.53
Pt	d_u	$CdAu_3$	(100)	Au	0.430	0.26
Pt	d_w	Cu_3Au	(110)	Au	0.500	0.39
Pt	d_c	Cu_3Au	(112)	Cu	0.505	0.38
Ir	d_c	$CuAu_3$	(112)	Cu	0.522	0.12
Ir	d_s	$CoPt_3$	(110)	Pt	0.541	0.41
Pt	d_c	$CoPt_3$	(110)	Pt	0.541	0.41
Ir	d_k	$CoPt_3$	(110)	Pt	0.541	0.41
Pt	d_k	$CoPt_3$	(110)	Pt	0.541	0.41
Pt	$\Delta\rho_t$	$CoPt_3$	(110)	Pt	0.541	0.41
Pt	d_s	$CoPt_3$	(110)	Pt	0.541	0.41
Ir	$\Delta\rho_t$	$CoPt_3$	(110)	Pt	0.541	0.41
Ir	$\Delta\rho_v$	$CoPt_3$	(110)	Pt	0.541	0.41
Pt	d_u	Pd_3Au	(112)	Au	0.568	0.06
Ir	d_s	Ag_3Pt	(100)	Pt	0.584	0.00
Pt	d_s	Ag_3Pt	(100)	Pt	0.584	0.00
Pt	d_c	$CuAu_3$	(100)	Cu	0.618	0.07
Ir	d_c	Cu_3PdAu_4	(102)	Cu	0.648	0.09
Ir	d_c	Cu_3PdAu_4	(211)	Cu	0.650	0.09
Ir	d_c	Cu_3PdAu_4	(102)	Cu	0.679	0.07
Pt	d_u	Cu_3PdAu_4	(102)	Au	0.684	0.06
Pt	d_w	Cu_3PdAu_4	(101)	Au	0.687	0.06
Pt	$\Delta\rho_v$	$NiPt_3$	(110)	Pt	0.694	0.12
Pt	d_w	$NiPt_3$	(110)	Pt	0.694	0.12
Pt	$\Delta\rho_t$	$NiPt_3$	(110)	Pt	0.694	0.12
Ir	$\Delta\rho_t$	$NiPt_3$	(110)	Pt	0.694	0.12

Ir	d_c	$NiPt_3$	(110)	Pt	0.694	0.12
Pt	d_w	Cu_3PdAu_4	(102)	Au	0.711	0.10
Ir	$\Delta\rho_v$	$CoPt_3$	(112)	Pt	0.799	0.11
Ir	$\Delta\rho_t$	$CoPt_3$	(112)	Pt	0.799	0.11
Pt	$\Delta\rho_v$	$CoPt_3$	(112)	Pt	0.799	0.11

8.3 Active sites for HER using NF pool

Table S8. Promising candidates for HER using NF pool sorted by the overpotential of HER (η_{HER}). Only the sites with $\eta_{HER} \leq 0.3V$ (considered successful predictions in this work) have been shown. The symbols for descriptors are the same as Table S6.

Ref	Descriptor	Bulk	Miller Index	Site	η_{HER} (V)	$E_{decomp,min}^{@E_{HER}^{0}-\eta_{HER}}$ (eV)
Pt	d_k	$NbCo_3$	(212)	Co	0.022	0.73
Ir	d_k	$NbNi_3$	(111)	Nb	0.124	0.48
Pt	d_s	$NbNi_3$	(111)	Nb	0.124	0.48
Pt	$\Delta\rho_t$	$NbCo_3$	(201)	Co	0.162	0.56
Ir	d_u	Zn_3Co	(120)	Co	0.200	0.26
Pt	d_w	$TaNi_6Mo$	(021)	Ni	0.241	0.26
Ir	d_w	Ni_3Mo	(001)	Ni	0.291	0.00
Pt	$\Delta\rho_v$	$CoNi_3$	(111)	Co	0.297	0.00
Pt	$\Delta\rho_t$	$CoNi_3$	(111)	Co	0.297	0.00
Pt	d_w	$NbNi_3$	(120)	Ni	0.298	0.27

8.4 Active sites for ORR using NF pool

Table S9. Promising candidates for ORR using NF pool sorted by the overpotential of ORR (η_{ORR}). Only the sites with $\eta_{ORR} \leq 0.8V$ (considered successful predictions in this work) have been shown. The symbols for descriptors are the same as Table S6.

Ref	Descriptor	Bulk	Miller Index	Site	$\eta_{ORR}\,(eV)$	$E_{decomp,min}^{@E_{ORR}^{0}-\eta_{ORR}}$ (eV)

Pt	d_u	ZnCu	(110)	Cu	0.564	1.20
Pt	d_u	Zn_2CuNi	(120)	Cu	0.673	1.05
Ir	d_c	$ZnCu_2Ni$	(211)	Cu	0.747	0.59
Ir	d_c	$ZnCu_2Ni$	(211)	Cu	0.747	0.59
Pt	d_c	Zn_2CuNi	(211)	Cu	0.779	0.96
Pt	d_u	ZnCu	(111)	Cu	0.785	0.77

9 Correlation between descriptors and overpotential

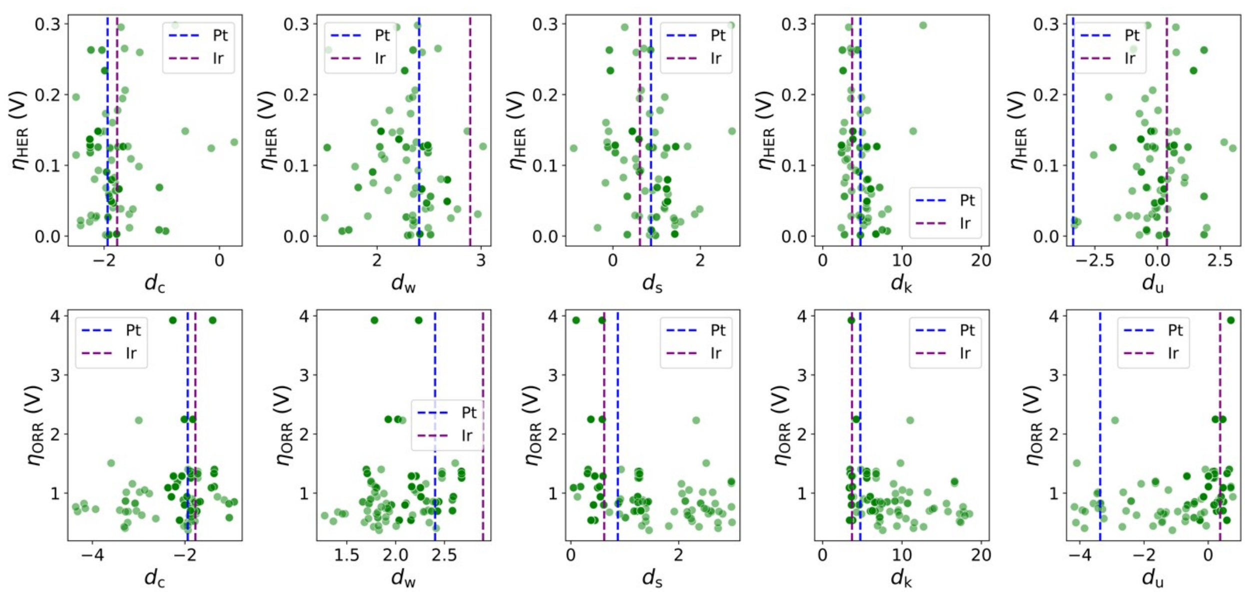

Figure S5. The correlation between investigated DOS-shape descriptors and the predicted overpotentials of HER (on the upper panels) and ORR (on the lower panels). The blue and purple dashed lines represent the values of descriptor for Pt(111) and Ir(111) surface sites.

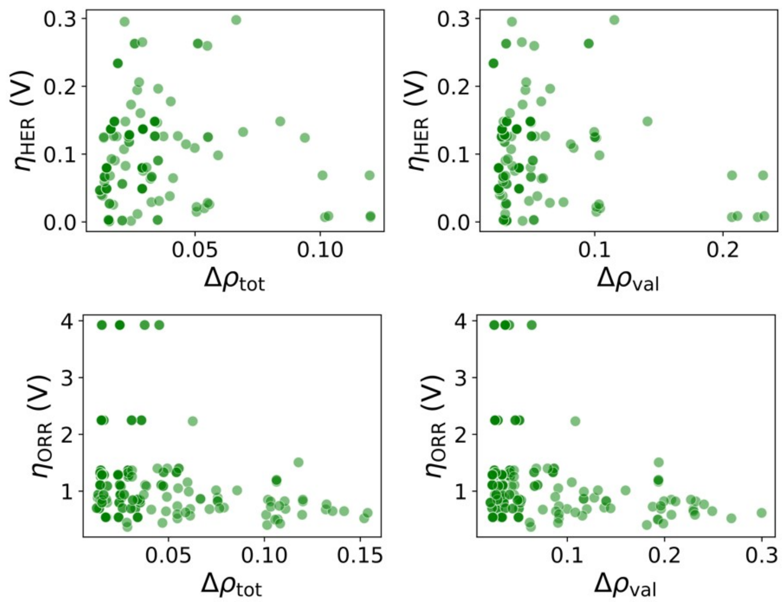

Figure S6. The correlation between investigated DOS-similarity descriptors and the predicted overpotentials of HER (on the upper panels) and ORR (on the lower panels).

10 Pourbaix diagram of promising candidates

10.1 HER candidates found using noble-metal-contained (NC) pool

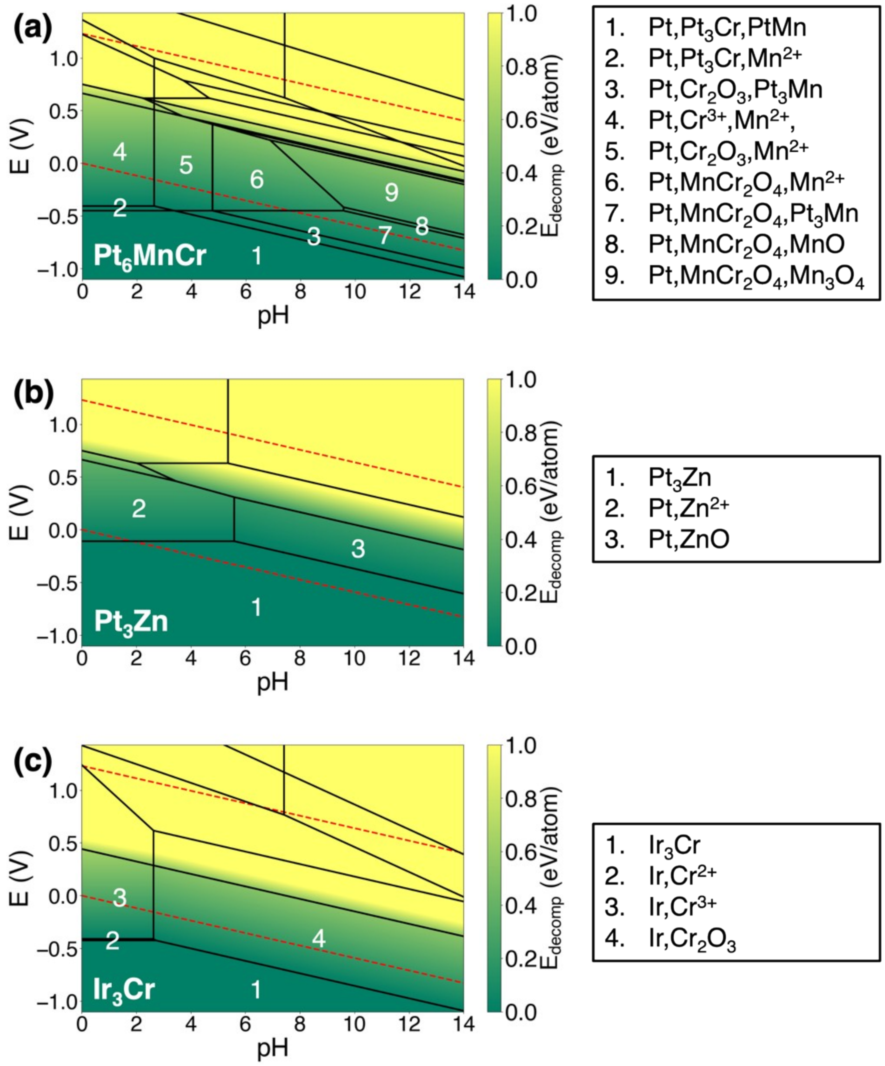

Figure S7. Pourbaix diagram of top three bulk phases of promising sites for HER shown in Fig. 7(a) using noble-metal-contained (NC) pool. The relevant regions for HER are labeled and their compositions are shown in the right box respectively. The compositions of the bulk phases were shown in the lower-left corner of each diagram.

10.2 HER candidates found using noble-metal-free (NF) pool

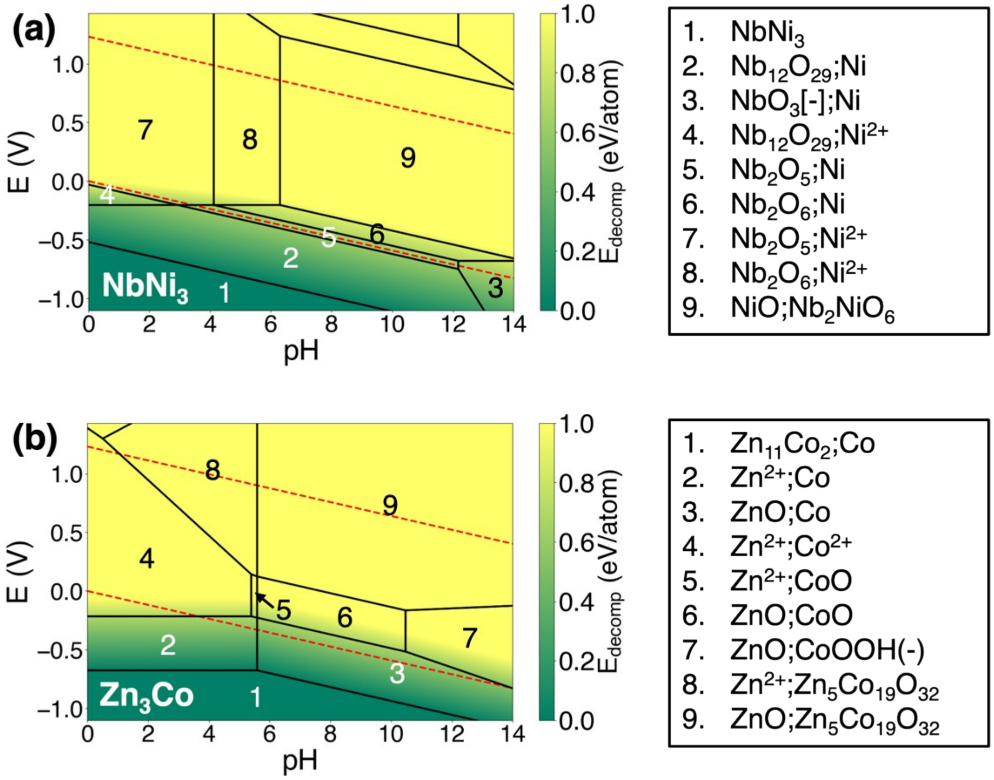

Figure S8. Pourbaix diagram of top three bulk phases of promising sites for HER shown in Fig. 7(a) using noble-metal-free (NF) pool. The $TaNi_6Mo$ case was excluded here because it has been shown in Fig. 7(b). The relevant regions for HER are labeled and their compositions are shown in the right box respectively. The compositions of the bulk phases were shown in the lower-left corner of each diagram.

10.3 ORR candidates found using noble-metal-contained (NC) pool

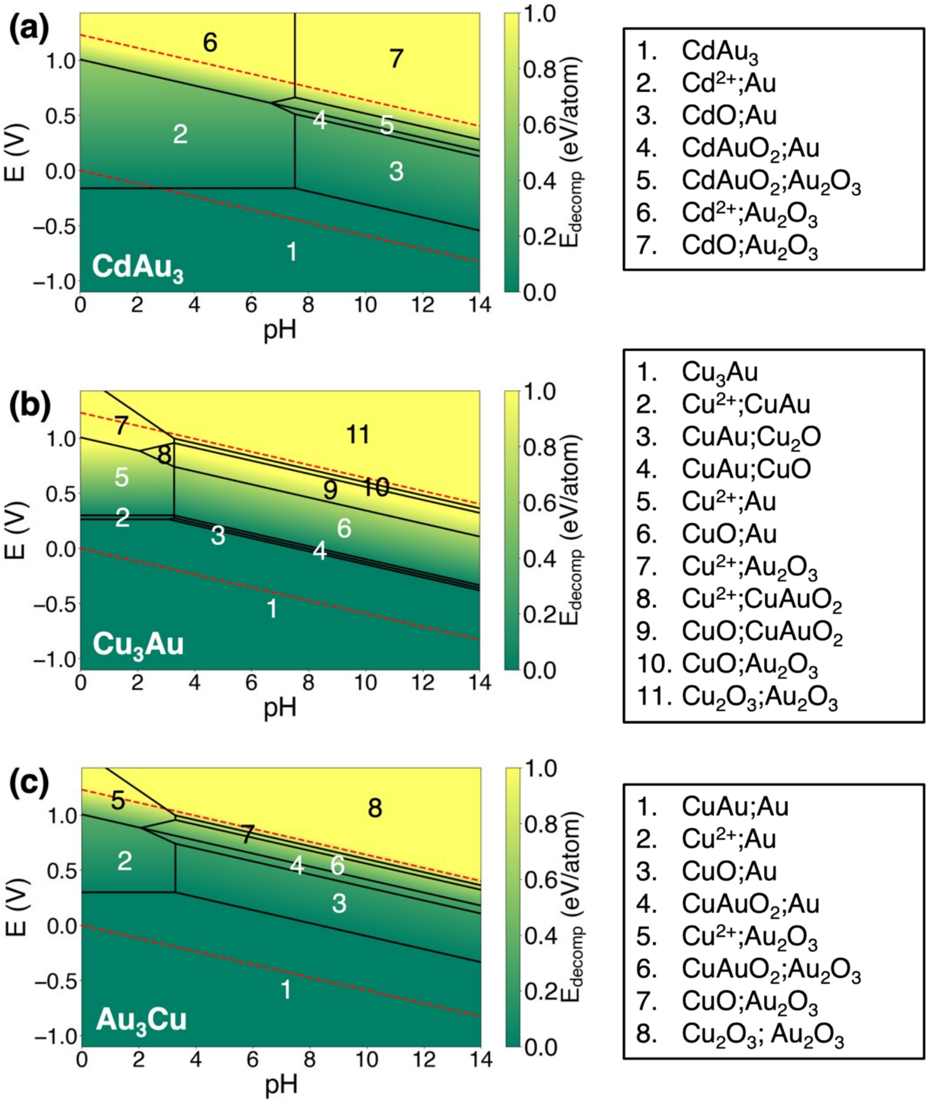

Figure S9. Pourbaix diagram of top three bulk phases of promising sites for ORR shown in Fig. 7(c) using noble-metal-contained (NC) pool. The relevant regions for ORR are labeled and their compositions are shown in the right box respectively. The compositions of the bulk phases were shown in the lower-left corner of each diagram.

10.4 ORR candidates found using noble-metal-free (NF) pool

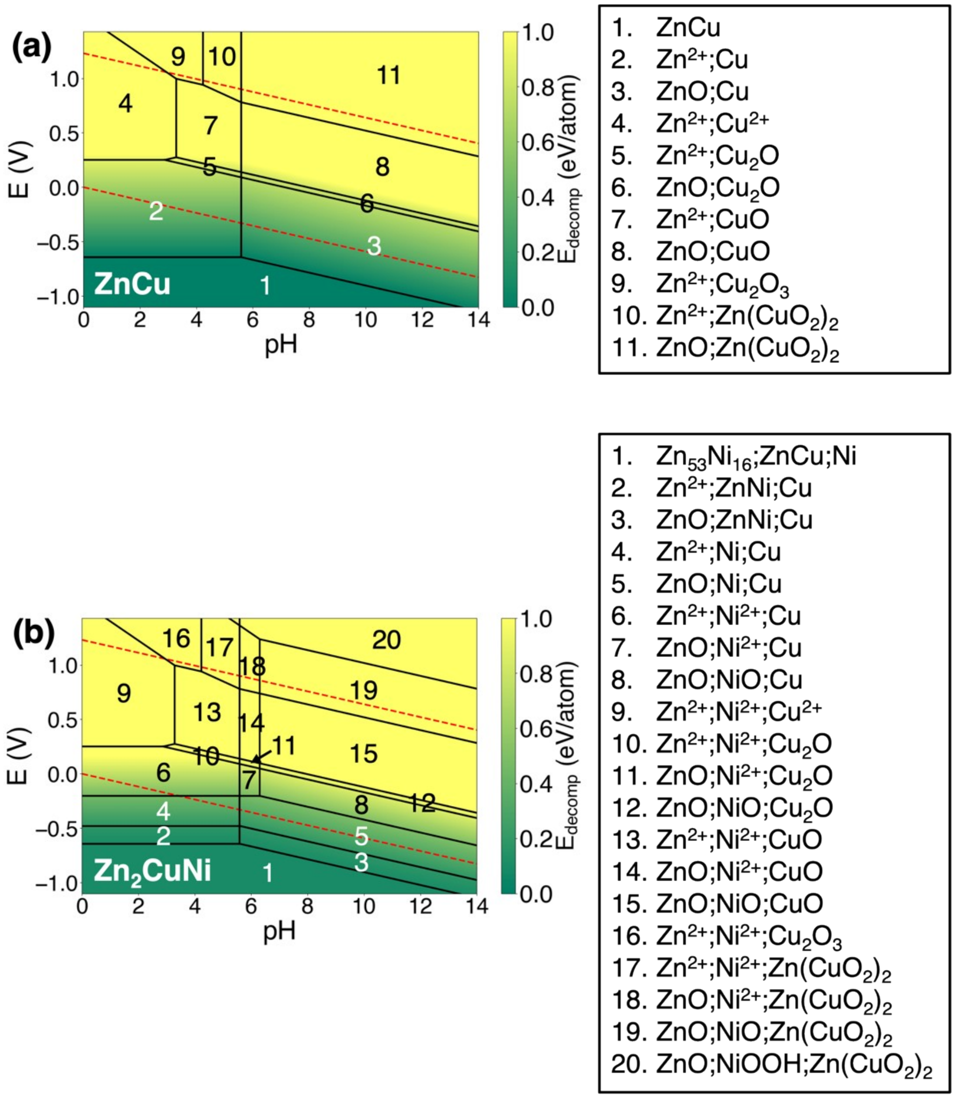

Figure S10. Pourbaix diagram of top three bulk phases of promising sites for ORR shown in Fig. 7(c) using noble-metal-free (NF) pool. The $ZnCu_2Ni$ case was excluded here because it has already been shown in Fig. 7(d). The relevant regions for ORR are labeled and their compositions are shown in the right box respectively. The compositions of the bulk phases were shown in the lower-left corner of each diagram.

11 Validation of simulation setting

To validate our simulation settings, we have compared our results of the adsorption energies of H (denoted as ΔG_{ads}^{H}) and overpotential of ORR (denoted as η_{ORR}) at Pt (111) and Ir (111) surfaces with previous works. All adsorbates (H/O/OH/OOH) are placed at top sites with coverage

$\theta_{ads} = 1/9ML$. Choosing top site is practical because our work is focused on comparing $\eta_{HER/ORR}$ of certain site with the reference surface according to the site-specific descriptors. It is also reasonable based on previous results. It is well documented in literature that the top-site H is active for HER.[14-17]. There is also a strongly adsorbed H on hollow site named "under-potential deposition H" (short as UPD-H). This distinction has been supported by both experiments[15, 18, 19] and simulations[14, 16, 17]. When the coverage of UPD-H bellows 0.7ML, the lateral interaction between UPD-H and OPD-H can be neglected, and the ΔG_{ads}^{H} of OPD-H is close to 0eV, which shows it is highly active for HER.[14] As for ORR, since the whole mechanism involves three adsorbates (O/OH/OOH), in order to get consistent result of overpotential on a single site, we only consider the top site adsorption for all adsorbates.

In our results, ΔG_{ads}^{H} at Pt (111) is -0.15eV, which is close to previous work(-0.16eV)[20, 21]. ΔG_{ads}^{H} on Ir (111) is -0.09eV, which is slightly higher than the value reported in the work by Greeley and Mavrikakis (-0.24eV, at $\theta_H = 0.25ML$)[21]. This observation is consistent with the work of Zhang and Li, where they showed that ΔG_{ads}^{H} for top-site H with low coverage on Ir (111) ($\theta_{H_{ads}} = 0.11ML$, which is the same as our case) has weaker adsorption, meaning ΔG_{ads}^{H} became more positive[22]. For η_{ORR} on Pt (111), our result (0.36V) is similar to 0.45V reported by Nøskov et al.[2]. For η_{ORR} on Ir (111), our result (0.62V) is slightly smaller than 0.85V reported by Nøskov et al.[2], which could result from different coverages of overpotential ($\theta_{OH} = 0.25ML$ in Ref. [2] and $\theta_{OH} = 0.11ML$ in our case). These comparisons illustrated the validity of our simulation settings.

Reference

1. J. K. Nørskov, T. Bligaard, A. Logadottir, J. Kitchin, J. G. Chen, S. Pandelov and U. Stimming, *Journal of The Electrochemical Society*, 2005, **152**, J23.

2. J. K. Nørskov, J. Rossmeisl, A. Logadottir, L. Lindqvist, J. R. Kitchin, T. Bligaard and H. Jonsson, *The Journal of Physical Chemistry B*, 2004, **108**, 17886-17892.
3. H. Xin, A. Vojvodic, J. Voss, J. K. Nørskov and F. Abild-Pedersen, *Phys. Rev. B*, 2014, **89**, 115114.
4. L. Fu, Y. Li, N. Yao, F. Yang, G. Cheng and W. Luo, *ACS Catal.*, 2020, **10**, 7322-7327.
5. I. Danaee and S. Noori, *International Journal of Hydrogen Energy*, 2011, **36**, 12102-12111.
6. F. Lv, J. Feng, K. Wang, Z. Dou, W. Zhang, J. Zhou, C. Yang, M. Luo, Y. Yang, Y. Li, P. Gao and S. Guo, *ACS Central Science*, 2018, **4**, 1244-1252.
7. Y. Xiao, L. Tang, W. Zhang and C. Shen, *Computational Materials Science*, 2021, **192**, 110402.
8. D. Chen, C. Li, H. Liu, F. Ye and J. Yang, *Scientific Reports*, 2015, **5**, 11949.
9. Z. Gao, S. Yun, C. Yang, Y. Zhang, J. Dang, G. Yang, T. Yang, D. Qiao and K. Wang, *Journal of Colloid and Interface Science*, 2023, **639**, 33-48.
10. Y.-Q. Yang, S.-J. Ji and N.-T. Suen, *Inorganic Chemistry*, 2023, **62**, 2188-2196.
11. D. N. Rodrigues-Júnior, N. G. Sousa, F. M. T. Luna, T. M. B. F. Oliveira, D. S. Abreu, W. Schwarzacher, P. de Lima-Neto and A. N. Correia, *Journal of Electroanalytical Chemistry*, 2023, **947**, 117785.
12. F. Qin, Z. Zhao, M. K. Alam, Y. Ni, F. Robles-Hernandez, L. Yu, S. Chen, Z. Ren, Z. Wang and J. Bao, *ACS Energy Letters*, 2018, **3**, 546-554.
13. R. Procaccini, S. Ceré and M. Vázquez, *Journal of Applied Electrochemistry*, 2009, **39**, 177-184.
14. E. Santos, P. Hindelang, P. Quaino, E. N. Schulz, G. Soldano and W. Schmickler, *ChemPhysChem*, 2011, **12**, 2274-2279.
15. I. Ledezma-Yanez, W. D. Z. Wallace, P. Sebastián-Pascual, V. Climent, J. M. Feliu and M. T. M. Koper, *Nature Energy*, 2017, **2**, 17031.
16. E. Skúlason, G. S. Karlberg, J. Rossmeisl, T. Bligaard, J. Greeley, H. Jónsson and J. K. Nørskov, *Physical Chemistry Chemical Physics*, 2007, **9**, 3241-3250.
17. M. T. Tang, X. Liu, Y. Ji, J. K. Norskov and K. Chan, *J. Phys. Chem. C*, 2020, **124**, 28083-28092.
18. B. E. Conway and B. V. Tilak, *Electrochimica Acta*, 2002, **47**, 3571-3594.
19. G. Jerkiewicz, *Progress in Surface Science*, 1998, **57**, 137-186.
20. M. J. Kolb, F. Calle-Vallejo, L. B. F. Juurlink and M. T. M. Koper, *The Journal of Chemical Physics*, 2014, **140**, 134708.
21. J. Greeley and M. Mavrikakis, *The Journal of Physical Chemistry B*, 2005, **109**, 3460-3471.
22. H. Zhang and W.-X. Li, *J. Phys. Chem. C*, 2009, **113**, 21361-21367.